Journal of Food Bioactives
International Society for Nutraceuticals and Functional Foods
Original Research
J. Food Bioact. 2024;000:000–000

Encapsulating *Salmo salar* byproduct-derived protein hydrolysate in chitosan/alginate nanoparticles

Janani Jayasinghe Mudiyanselage[a,b,c], Thilini Dissanayake[a,b], Aishwarya Mohan[c], Beth Mason[c*] and Nandika Bandara[a,b*]

[a]Department of Food and Human Nutritional Sciences, Faculty of Agricultural and Food Sciences, University of Manitoba, Winnipeg, MB. R3T 2N2. Canada
[b]Richardson Center for Food Technology and Research, 196 Innovation Drive Winnipeg, MB R3T 2N2 Canada
[c]Verschuren Center for Sustainability in Energy and Environment, 1250 Grand Lake Rd, Sydney, NS B1M 1A2 Canada
[*]**Corresponding author:** Beth Mason, Verschuren Center for Sustainability in Energy and Environment, 1250 Grand Lake Rd, Sydney, NS B1M 1A2 Canada., E-mail: bmason@verschurencentre.ca; Nandika Bandara, Department of Food and Human Nutritional Sciences, Faculty of Agricultural and Food Sciences, University of Manitoba, Winnipeg, MB. R3T 2N2. Canada.E-mail: Nandika.Bandara@umanitoba.ca
DOI: 10.31665/JFB.20xx.000xx
Received: June 25, 2024; **Revised received & accepted:** August 23, 2024
Citation: Mudiyanselage, J.J., Dissanayake, T., Mohan, A., Mason, B., and Bandara, N. (2024). Encapsulating *Salmo salar* byproduct-derived protein hydrolysate in chitosan/alginate nanoparticles. J. Food Bioact. 000: 000–000.

Abstract

Byproducts-derived protein hydrolysates are known to have different bioactivities such as antioxidative, antihypertensive, antidiabetic, immunomodulatory, and antiproliferative activities that help improve human health. Low bioavailability, stability, heterogenous nature, interaction with food matrix, and hydrophobicity limit their applications. Hence, nanocarriers could be an effective method of delivering these hydrolysates. This study aimed to develop and optimize chitosan/alginate nanoparticles (CS/AL NPs) to deliver *Salmo salar* by-product-derived protein hydrolysates (SPH). The optimized nanoparticle size, zeta potential, and encapsulation efficiency (EE) were 536.7 nm, −30.2 mV, and 29.8%, respectively. XRD and FTIR results proved the incorporation of SPH into the CS/AL NPs. Moreover, the release of SPH in the salivary phase is higher due to the high amount of free SPH in the nanoparticle suspension. Encapsulated SPH was protected in the gastric phase and showed a controlled release in the intestinal phase. The ultimate goal of utilizing these nanoparticles is to fabricate functional food products, and thereby offer consumers greater health benefits through the bioactive properties of hydrolysates.

Keywords: Bioactivity; Encapsulation; Controlled-release; *Salmo salar* byproduct; Chitosan; Alginate.

1. Introduction

Bioactive peptides are recognized as promising functional food ingredients that can be incorporated into foods to attain health-promoting activities. These bioactive peptides are well known to play an essential role in human health by providing properties like antioxidative, antihypertensive, antidiabetic, immunomodulatory, and antiproliferative (Bhandari et al., 2020; Aguilar-Toalá et al., 2022). The biological activity of the peptides depends on their amino acid sequence and composition. Usually, bioactive peptides contain 2–20 amino acid residues (Sarabandi et al., 2020). Bioactive peptides can be derived from various food sources, including plants, animals, and agro-processing industry byproducts. During food processing, significant amounts of byproducts are generated, causing problems in disposal (Bhandari et al., 2020; Görgüç et al., 2020). In particular, disposing of marine or fish-derived byproducts in the environment is problematic. In 2022, global fish production was 223.2 million tons, according to the Food and Agriculture Organization's (FAO) world fishery and aquaculture statistics (FAO, 2022). Fish processing generally yields up to 45% (per carcass weight) of byproducts, which include viscera, trimmings, heads, and backbone. However, these byproducts can be an excellent source for producing valuable functional food

ingredients and nutraceuticals such as bioactive peptides. *S. salar* is the leading aquaculture species produced in Canada and ranked fourth in the world in production volumes (DFO, 2022). Hence, large amounts of byproducts are generated during the processing of salmon in Canada which make up 60% of the total output (Ramakrishnan et al., 2024). As these byproducts contain a considerable amount of protein (10–20% w/w), they could be used as a cheap source to generate protein hydrolysates and peptides with biological activities beneficial for humans (Zamora-Sillero et al., 2018). Researchers have identified protein hydrolysates and peptides with varied bioactivities from salmon byproducts (Gao et al., 2021).

However, the application of these bioactive peptides in the food industry has been restricted due to their low stability in gastrointestinal digestion, low bioavailability, bitter taste, hydrophobicity, interactions with other food compounds, and hygroscopicity, thereby losing their health benefits. Accordingly, encapsulation could be employed for bioactive peptides derived from various food sources as a potential solution for commercial food production (Aguilar-Toalá et al., 2022). Different delivery agents have been developed to encapsulate bioactive ingredients, including lipids, proteins, and polysaccharides (Shishir et al., 2018). The delivery agents should be able to protect the bioactive agents and improve their stability and bioavailability. Different encapsulation systems could be used to deliver bioactive proteins and peptides such as liposomes, solid lipid nanoparticles (SLNs), biopolymer microgels, water in oil emulsions, water in oil in water (W/O/W) emulsions, W/O/W–SLNs and emulsified microemulsions (Perry and McClements, 2020). Among them, polysaccharides have attracted much attention as encapsulation material. The growing interest in using polysaccharides as an encapsulating material for bioactive compounds has emerged due to their beneficial characteristics such as higher biodegradability, biocompatibility, higher structural flexibility, hydrophilicity, diverse physicochemical properties, readily available and safe to humans (Aguilar-Toalá et al., 2022).

Alginate and chitosan are bio-polysaccharides, and both are extracted from marine sources. Chitosan and alginate encapsulate different bioactive compounds, including vitamins, phenols, carotenoids, proteins, essential oils, etc. (Li et al., 2021). Both polymers are widely used as encapsulation agents due to their desirable properties that were stated earlier. Chitosan (positively charged) and alginate (negatively charged) are oppositely charged polymers. The stability of alginate is high in acidic conditions, while stability is low in alkaline conditions. In contrast, chitosan is unstable in an acidic environment, one of the major barriers despite all other beneficial properties. Therefore, researchers attempted to achieve synergistic effects from both polymers by combining two polymers via electrostatic interactions, which allowed them to obtain a controlled release of bioactive compounds in the gastric environment (Nalini et al., 2019). Chitosan/alginate nanoparticles have been used for the oral delivery of different bioactive compounds, including enoxaparin, curcumin, naringenin, insulin, quercetin, BSA, etc. (Li et al., 2021). However, the application of chitosan and alginate nanoparticles to deliver heterogeneous protein hydrolysates and peptides is still limited in the literature. Hence, this study hypothesizes that the salmon byproducts derived protein hydrolysates encapsulated chitosan/alginate nanoparticles (CS/AL NPs) will sustain hydrolysates' release in the gastric environment. This study aimed to optimize the process conditions for CS/AL NPs preparation and characterize the prepared nanoparticles. Finally, the release behavior in simulated gastrointestinal conditions will be studied.

2. Materials and methods

2.1. Materials

Low molecular weight chitosan (50–190 KDa, 75–85% deacetylated), Alginate, Pepsin from porcine gastric mucosa, Pancreatin from porcine pancreas, Alpha-amylase from porcine pancreas was purchased from Sigma-Aldrich (Wisconsin, USA). Bile extract was purchased from Santa Cruz Biotechnology, Inc. (Dallas, USA). Other chemicals that were applied were of analytical grade and purchased from Thermo Fisher Scientific, Ottawa, Canada.

2.2. Preparation of S. salar protein hydrolysates

The SPH was prepared by following the method described previously (Rajendran et al., 2018). Briefly, the byproducts from Atlantic salmon (*S. salar*) processing were obtained and frozen for future use. The byproducts, mainly the offal, were obtained from market-size salmon which were processed into Head On Gutted (HOG) fish. Before fermentation, the byproducts were thawed and blended to obtain a uniform mix (slurry). A batch fermenter (New Brunswick Bioflow/CelliGen 115, GMI, Inc., MN) was used to ferment the blended *S. salar* byproduct slurry. The fermentation was initiated by adding deproteinized whey (5% w/w) (80–90% lactose) and lactic acid (1%) bacteria inoculum to the byproduct slurry of 750 g. The fermentation conditions were set to 37 °C (temperature) and 150 rpm (agitation) and allowed to ferment for 2 days. After fermentation, the resulting slurry was centrifuged (3,500 × g for 15 min) to separate the different fractions. Then, separated SPH was further fractionated according to their molecular weight using an Amicorn ultrafiltration stirred cell (Millipore Corp., Billerica, MA, USA). A 1 kDa and 10 kDa ultrafiltration membranes were used to obtain the 1–10 kDa SPH fraction. After the fractionation, all SPH samples were freeze-dried and stored at −20 °C until further use.

2.3. Preparation of S. salar fermentative protein hydrolysates (SPH) encapsulated chitosan/alginate nanoparticles

Chitosan/alginate nanoparticles (CS/AL NPs) were prepared according to the method described by Mukhopadhyay et al. with slight modifications for alginate concentration, $CaCl_2$ concentration, and sonication time (Mukhopadhyay et al., 2015). Briefly, the alginate solution was prepared at a 1.5 mg/ml concentration in distilled water, and the pH was adjusted to 5.1. Next, the chitosan solution was prepared in a separate beaker by dissolving chitosan in 1% acetic acid at a 3 mg/ml concentration, and the pH was adjusted to 5.5. The SPH solution was prepared by dissolving the SPH peptide fraction (1–10 KDa) in 10 mM phosphate buffer (5 mg/ml). Chitosan/alginate nanoparticles were prepared using a two-step method. First, aqueous $CaCl_2$ (1.5 mg/ml) and peptide solution were mixed. This was then added dropwise to an aqueous solution of alginate and then sonicated for 10 min using a probe sonicator (Fisherbrand™ Model 505 Sonic Dismembrator, Thermo Fisher Scientific, USA). Then, the previously prepared chitosan solution was added dropwise to the calcium alginate pre-gel, and sonicated for another 15 min. The resulting opalescent suspension was kept overnight (at room temperature) to obtain uniform particles.

2.4. Experimental design

Chitosan/alginate nanoparticle formation was optimized using a

Table 1. Codes and levels of independent variables used for the optimization

Codes	Independent variables	Levels		
		Low (−1)	Medium (0)	High (+1)
X_1	Alginate/Chitosan (w/w) (AL/CH)	2	5	8
X_2	Alginate/$CaCl_2$ (w/w) (AL/$CaCl_2$)	4	5	6
X_3	Alginate/peptides (w/w) (AL/SPH)	1	2	3

Box-Behnken design to select the best conditions and input variables. Three independent variables, AL/CH (w/w), alginate/ $CaCl_2$ (w/w), and alginate/peptides (w/w), were optimized where a range of levels were tested as indicated in Table 1. The response surface methodology (Box-Behnken design) with 15 experimental combinations (in triplicate) was used to optimize the conditions for nanoparticle formation where particle size (nm) and encapsulation efficiency (%) of the nanoparticles were considered as the dependent variables. The experimental conditions were optimized for smaller particle sizes and higher encapsulation efficiency.

The polynomial equation for the design is given below.

$$Y = \beta_O + \beta_1 X_1 + \beta_2 X_2 + \beta_3 X_3 + \beta_{12} X_1 X_2 + \beta_{13} X_1 X_3 + \beta_{23} X_2 X_3 + \beta_{11} X_1^2 + \beta_{22} X_2^2 + \beta_{33} X_3^2 \quad (1)$$

Where Y is the dependent variable, β_O is the intercept coefficient, β_1 to β_{33} are the regression coefficients, X_1, X_2, and X_3 are coded levels of independent variables, and X_1, X_2, and X_i^2 (i = 1, 2, or 3) are interaction and interaction and quadratic terms respectively.

2.5. Characterization of nanoparticles

2.5.1. Particle size, Polydispersity index (PDI), and zeta potential

A Zeta potential analyzer (ZetaPALS, Brookhaven Instruments, New York, USA) based on dynamic light scattering technology was used to measure the particle size, PDI, and zeta potential. The samples were characterized using the original samples without dilution (5 runs per replicate).

2.5.2. Encapsulation efficiency (EE)

The EE of the fractionated SPH hydrolysates (1–10 kDa) was determined based on the methods described by Du et al. with slight modification (Du et al., 2019). The initial fermented SPH was fractionated using Amicon Ultra centrifugal filters (VWR International, PA, USA) with a 10 kDa molecular weight cut-off. Then, about 0.5 mL of nanoparticle suspension was transferred into the centrifugal filter and centrifuged for 10 min at 4,000 rpm. The supernatant was collected, and the unencapsulated SPH in the filtrate was determined using the Lowry protein assay kit. EE was calculated based on the following Equation 2.

$$EE\ (\%) = \frac{\text{Total amount of peptide} - \text{Free amount of peptide}}{\text{The total amount of peptide}} \times 100 \quad (2)$$

The morphology of the blank CS/AL NPs and SPH-loaded CS/AL NPs were characterized using Transmission electron microscopy (TEM). First, a drop of nanoparticle suspension was deposited in a 300-mesh carbon film-coated grid. Then, the staining was done by adding 1% uranyl acetate solution to the grid with samples. The excess solution was removed using filter paper. Finally, the grid was air-dried properly before imaging using the TEM (Mohan et al., 2018).

2.5.4. Fourier transform infrared spectroscopy (FTIR)

The chemical interactions of the nanoparticles and their precursor compounds were identified using Fourier transform infrared spectroscopy (FTIR) spectra (Nicolet 6700 FTIR, Thermo Electron Inc, Madison, WI, USA). FTIR spectra for the chitosan, alginate, SPH, blank CS/AL NPs, and SPH-loaded CS/AL NPs were obtained at room temperature in the 4,000 to 400 cm^{-1} wavelength range. OMNIC software was used to collect the spectra at 120 scans and a spectral resolution of 4 cm^{-1} (Mukhopadhyay et al., 2015).

2.5.5. X-ray diffraction (XRD)

X-ray diffraction analysis was performed for chitosan, alginate, SPH, freeze-dried blank CS/AL NPs, and SPH-loaded CS/AL NPs to study the crystallinity of the initial compounds and prepared nanoparticles. The study used a Siemens/Bruker X-ray diffractometer (D5000, BrukerNano Inc, Madison, WI, USA) with a Cu X-ray tube. A quartz sample holder was used to place the samples, and scanning was done at a diffraction angle of 2θ from 3–60° in step-scan mode using a 0.02° step and 1s dwell time.

2.6. Release during simulated gastrointestinal digestion

The release of SPH from the CS/AL NPs was evaluated using a digestion model described by Flores et al. and Giroux et al. with slight modifications (Flores-Jiménez et al., 2019; Giroux et al., 2019). The digestion conditions are mimicked to match the composition of saliva, gastric, duodenal, and bile extracts. The exact compositions of the digestion solutions are listed in Table 2. Moreover, sequential digestion was conducted for the optimized nanoparticles and free hydrolysates.

For the simulated saliva digestion, 2.5 g of nanoparticles were mixed with 3 mL of salivary juice in a Falcon tube and was mixed in a water bath (Model 1227, VWR International, Cornelius, OR, USA) at 37 °C for 10 min at 200 rpm. The gastric digestion was carried out for the resulting saliva digest, where 6 mL of gastric juice was added, and digestion was done for 2 hrs at 37 °C (200 rpm) in a water bath. The pH of the mix was adjusted to 3 using 1 M HCl during the digestion. For intestinal digestion, 6 mL of duodenal juice and 3 mL of bile juice were added to the gastric digesta. Mixing was done for another 2 hrs at 37 °C for 10 min at 200 rpm. The pH of the mixture was adjusted to pH 7–7.2. pH using 1 M NaOH.

During each digestion phase, samples were collected at differ-

Table 2. Composition of simulated gastrointestinal fluids (Flores et al., 2014)

Saliva stock solution	Gastric stock solution	Duodenal stock solution	Bile stock solution
200 mL of milliQ water	200 mL of milliQ water	200 mL of milliQ water	250 mL of milliQ water
23.4 mg NaCl	1.10 g NaCl	2.80 g NaCl	2.10 g NaCl
29.8 mg KCl	0.33 g KCl	0.23 g KCl	0.15 g KCl
0.42 g $NaHCO_3$	0.11 g $NaHPO_4$	1.36 g $NaHCO_3$	2.31 g $NaHCO_3$
0.08 g of Urea	0.16 g $CaCl_2{\cdot}2H_2O$	32 mg KH_2PO_4	0.10 g Urea
	0.12 g NH_4Cl	20 mg $MgCl_2$	0.06 mL Conc. HCl
	0.03 g Urea	0.04 g Urea	
	2.6 mL Conc. HCl	0.0 mL Conc. HCl	
0.4 g Amylase	1 g Pepsin	3.6 g Pancreatin	12 g Bile extract
pH 6.8 ± 0.2	pH 1.3 ± 0.02	pH 8.1 ± 0.2	pH 8.2 ± 0.2

ent time intervals. For example, samples were collected at 0 and 10 min during salivary digestion and 30, 60, 90, and 120 min during gastric and intestinal digestion. About 0.5 mL of digestive was transferred into the centrifugal filter and centrifuged at 4,000 rpm for 10 min. The release rate was calculated in comparison to the release of free SPH in gastrointestinal digestion. The release of the SPH from the CS/AL NPs was determined using the Lowry protein assay kit.

2.7. Statistical analysis

Minitab (version 19, Minitab Inc., Pennsylvania, USA) and Origin 2021 (OriginLab Corporation, USA) were used for the statistical analysis. The Significance level used was 5% for the Analysis of Variance (ANOVA).

3. Results and discussion

3.1. Optimization of nanoparticle preparation

3.1.1. Variance analysis

The response surface methodology (RSM) optimized encapsulation used a Box Behnken design with 15 factorial points and 3 center points (3 replicates). The particle size of the SPH-loaded CS/AL NPs ranged from 440.50 nm to 3.92 µm, where zeta potential ranged from −20.03 to −33.63 mV. Similarly, the EE of the prepared samples varied from 3.62 to 43.57 w/w %. Analysis of variance was used to fit the model for three independent variables. Backward elimination (0.1) was performed to remove the non-significant terms in the model. As a result, all the three-parameter models were significant, showing the best fit (Table 3). Moreover, closer R^2 and adjusted R^2 for the three response variables depict the adequacy of the derived models and indicate the ability to predict the corresponding responses. Although the particle size and zeta potential are within acceptable ranges, the low encapsulation efficiency reveals a limitation of this encapsulant system. Exploring alternative encapsulant systems, such as double emulsions, could improve encapsulation efficiency. However, this study only focused on nanoparticles.

The regression equations for each response variable were as follows.

$$\text{Particle size (nm)} = -4693 - 380X_1 + 2395X_2 + 541X_3 + 69.3X_1X_1 - 248X_2X_2 + 293X_3X_3 - 266.9X_1X_3 \quad (3)$$

$$\text{Zeta potential (mV)} = -14.03 - 5.404X_1 + 0.35X_2 + 5.12X_3 + 0.4353X_1X_1 - 1.059X_2X_3 \quad (4)$$

$$\text{Encapsulation Efficiency (\%)} = 157.4 - 10.14X_1 - 65.1X_2 + 28.89X_3 + 0.327X_1X_1 + 6.59X_2X_2 + 3.61X_3X_3 + 1.765X_1X_2 - 1.599X_1X_3 - 4.41X_2X_3 \quad (5)$$

When considering the model terms for particle size, X_1, X_2, X_3 (linear terms), X_1X_1, X_2X_2, X_3X_3 (square terms), and X_1X_3 (2-way interaction terms) were all significant according to the ANOVA Table 3. X1, X2 (linear terms), and X1X1 (square terms) were significant for the zeta potential. Lastly for the encapsulation efficiency, X_1, X_3 (linear terms), X_1X_1, X_2X_2, X_3X_3 (square terms) and X_1X_2, X_1X_3, and X_2X_3 (2-way interaction terms) were highly significant. These observations align with the formation of CS/AL NPs based on the electrostatic interactions between two oppositely charged polymers.

3.1.2. Effects of independent variables on particle size

The particle size of the SPH-loaded CS/AL NPs ranged from 440.50 nm to 3.92 µm. According to the ANOVA for particle size, it was significantly affected by both three independent variables and the interaction between the AL/CH ratio and AL/SPH ratio

Table 3. Summary of the ANOVA table

Response	Significance	R^2	Adjusted R^2	Predicted R^2
Particle size	0.000	0.8301	0.7979	0.7267
Zeta potential	0.000	0.7807	0.7526	0.6925
Encapsulation efficiency (EE)	0.000	0.8981	0.8718	0.8205

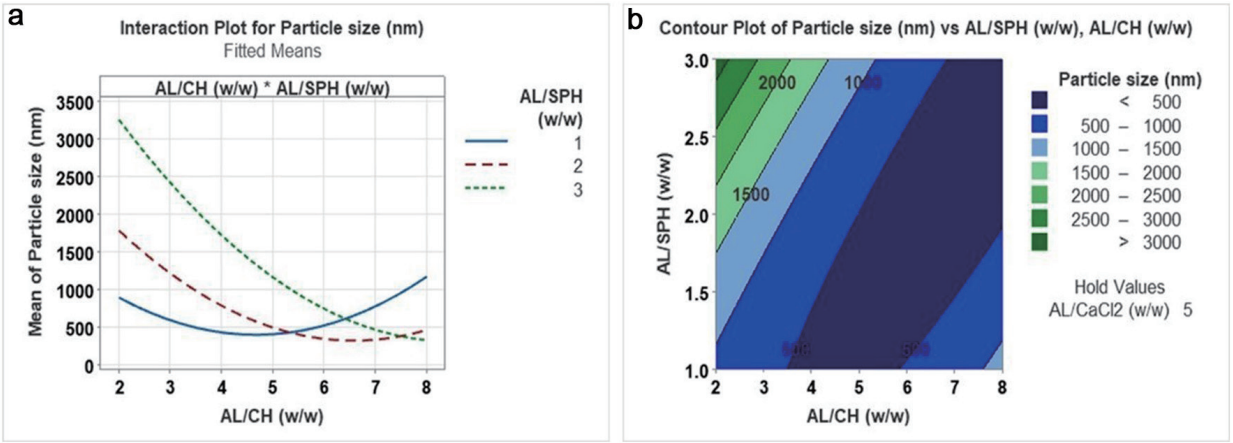

Figure 1. Interaction plot (a) and contour plot (b) for the effect of AL/CH (alginate/chitosan) (w/w) versus AL/SPH (alginate/ S. salar by-product-derived protein hydrolysates) (w/w) on particle size.

(Figure 1). Particle size was increased with the reduction of the AL/CH ratio, and particle size of the nanoparticles was increased with increasing AL/$CaCl_2$ ratio. Moreover, the nanoparticles' particle size increased with the AL/SPH ratio. It could be observed that the lowest particle size (<500 nm) was recorded between 4 to 6 of the AL/CH ratio. CS/AL NPs are formed based on the electrostatic interactions between two oppositely charged polymers where alginate will be crosslinked with calcium ions through ionic gelation to form an egg-box structure with a pre-gel state. The cationic chitosan (NH_3^+) will be added to the pre-gel to form a polyelectrolyte complex with the anionic alginate (COO^-) (Zimet et al., 2018). The number of electrostatic interactions between the alginate (anionic) and chitosan (cationic) will determine the size of the particles, i.e. if these are low, then particle size is increased. This is due to the available amino groups in the chitosan that inhibit the crosslinking reactions (Rahaiee et al., 2015; Zhang and Kosaraju, 2007). Similar results have been observed for curcumin diethyl disuccinate encapsulated with chitosan/alginate nanoparticles. Particle size was increased from 281 nm to 414 nm with an increased chitosan/alginate ratio from 0.05:1 to 0.15:1 while increasing beyond 0.15:1 resulted in aggregation and an opaque solution (Bhunchu et al., 2015).

3.1.3. Effect of independent variables on zeta potential

Zeta potential is an important parameter in determining the formed nanoparticles' stability and reflects the particles' surface charge in a solution or a suspension. A higher surface charge is preferred in a system that can prevent the aggregation of the particles through repulsive forces (Sorasitthiyanukarn et al., 2018). A zeta potential above +30 mV or below −30 mV provides good stability to particles in a colloidal system due to adequate repulsive forces (Azevedo et al., 2014). In this study, the zeta potential of the prepared nanoparticles ranged from −20.03 to −33.63 mV. The AL/CH ratio and Alginate/CaCl2 ratio significantly affected Zeta potential among the parameters tested. All the nanoparticles prepared during the optimization study showed a negative zeta potential due to the high proportion of alginate. The AL/CH ratio showed an antagonistic effect on the zeta potential, where a reduction of the zeta potential was observed with the increase of the ratio from 2 to 8. At a higher chitosan level in the suspension, the less negative zeta potential was observed as cationic chitosan was predominantly present to make electrostatic interactions with alginate. Similar patterns for zeta potential have been observed by Ji's group (Ji et al., 2019) for cinnamaldehyde-encapsulated chitosan/alginate nanoparticles, where a lower zeta potential was observed at an AL/CH ratio of 6 in a single-factor experiment. In another study by Hosseini and Varidi, rennet-encapsulated AL/CH nanoparticles showed similar findings. Higher amounts of alginate caused an increase in zeta potential from −13 to −21 mV, and with the increase of chitosan, zeta potential values went up to +27 mV. The cationic nature of the chitosan leads to this positive zeta potential (Hosseini and Varidi, 2021).

AL/$CaCl_2$ ratio showed a synergistic effect on the zeta potential. A higher concentration of $CaCl_2$ in the system may neutralize the -COO^- group in alginate by Ca^{2+} (Chandrasekar et al., 2017; Ji et al., 2019). In an optimization study conducted to encapsulate nisin using chitosan and alginate nanoparticles, the zeta potential was significantly affected by the independent variables (alginate concentration, AL/CH (w/w), and Nisin concentration). However, the optimized nanoparticles had a zeta potential of −31.7 ± 2.6 mV (Zimet et al., 2018); however, in this study, the SPH amount in the suspension did not significantly affect the zeta potential.

3.1.4. Effect of independent variables on EE

EE of the SPH-loaded CS/AL NPs was significantly affected by AL/CH and AL/SPH ratios. The relationship between the independent variables and EE is shown in Figure 2 using interaction plots and contour plots, respectively. As shown in Figure 2a and b, higher EE of SPH was observed at an AL/CH ratio of around 2. In contrast, the highest EE (>25%) was recorded when AL/CH and alginate/$CaCl_2$ ratios were 2 and 4, respectively. According to Figure 2c–f, it is evident that the EE decreased as the AL/SPH ratio decreased in the nanoparticles, irrespective of the AL/CH and AL/$CaCl_2$ ratios. Higher SPH content in the nanoparticles resulted in lower EE. This may result from the SPH overload within the polymer matrix, leading to a release of the excess SPH from the polymer matrix that was unable to be kept within the nanoparticle system (Honary and Zahir, 2013; Sorasitthiyanukarn et al., 2018). In contrast, Rahaiee et al., (2015) found that high concentrations of polymers may form a bulk matrix of nanoparticles, thereby reducing the space for the material encapsulated in the matrix (crocin). Bhunchu and the group reported an increase in the EE (from 33.2 to 54.9%) of the curcumin diethyl di-succi-

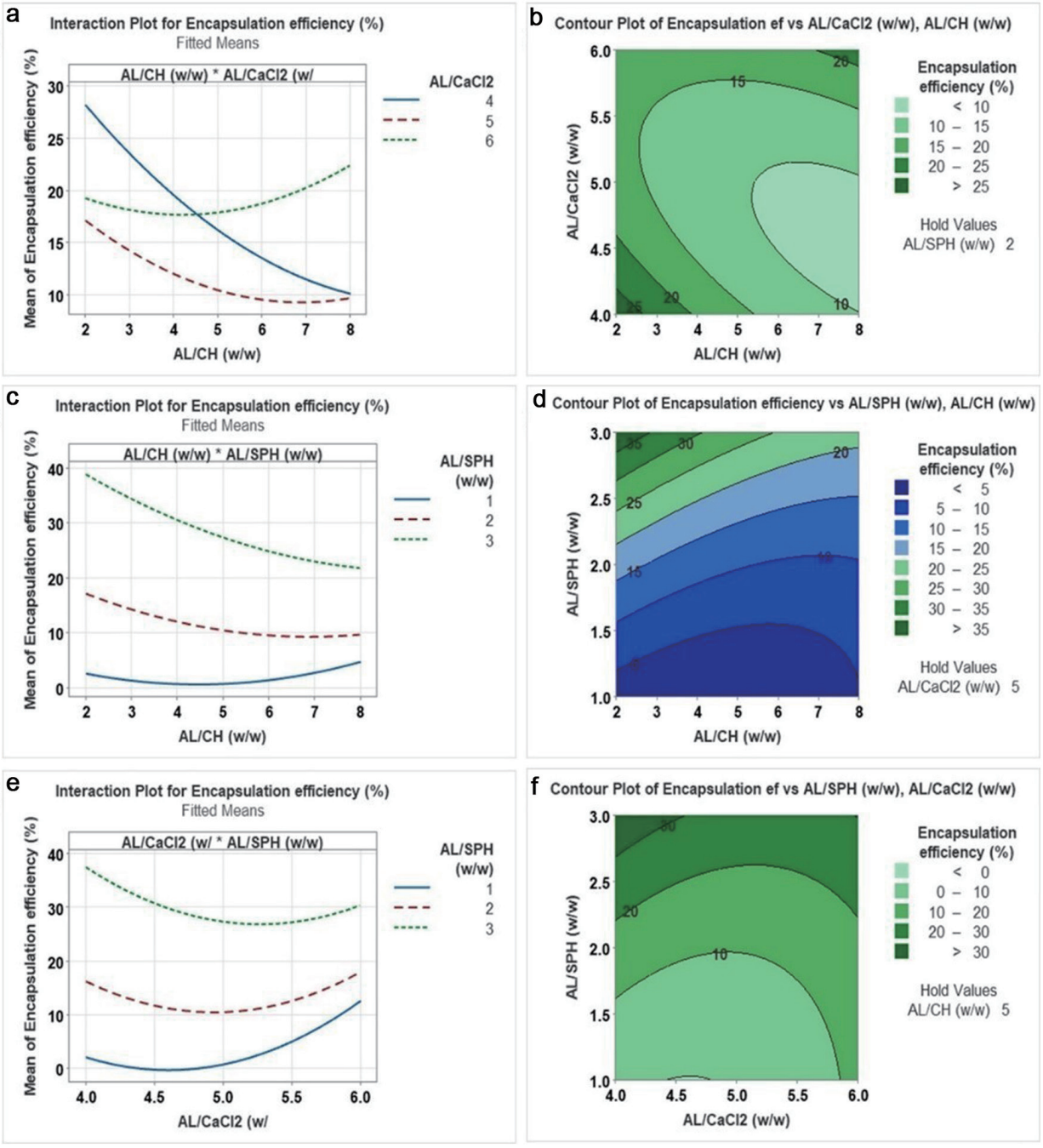

Figure 2. Interaction plot and contour plot for the effect of (a), (b) AL/$CaCl_2$ (w/w) versus AL/CH (w/w): (c), (d) AL/SPH (w/w) versus AL/CH (w/w): (c), (d) AL/SPH (w/w) versus AL/CaCl2 (w/w) on encapsulation efficiency. AL = alginate, CH = chitosan, SPH = S. salar by-product-derived protein hydrolysates.

nate when the chitosan/alginate ratio was increased from 0.05:1 to 0.15:1 (Bhunchu et al., 2015).

3.2. Validation of optimized nanoparticle preparation conditions

The optimized conditions were validated by conducting five independent experiments using the optimum conditions generated from the RSM optimization. When performing the response optimization, particle size and zeta potential were optimized to a minimum, while EE was optimized to a maximum. The optimized conditions that were generated from the model are AL/CH (w/w): 6, AL/$CaCl_2$ (w/w): 6, and AL/SPH(w/w): 3. The predicted generated from the RSM model and experimental values observed from the validation study for responses are shown in Table 4. When comparing the predicted and experimental values, the experimental zeta potential and EE values were very close to the predicted values. Although

Table 4. Predicted and experimental values for responses: particle size, zeta potential, and Encapsulation efficiency

Response variable	Predicted value	Experimented value	95% Confidence Interval
Particle size (nm)	417	536.70 ± 21.20	(87, 748)
Zeta potential (mV)	−32.4	−30.22 ± 0.88	(−36.621, −28.179)
EE (%)	29.63	29.80 ± 4.5	(19.49, 39.78)

the experimental particle size was higher than the predicted value, it falls within the accepted confidence interval (87,748 nm) for the particle size generated from the model. Also, the PDI (0.239 ± 0.028) for the optimized nanoparticles was less than 1, indicating the narrow particle size distribution. A zeta potential value of −30.22 mV depicts the higher stability of the formed nanoparticles in the suspension. EE of the formed nanoparticles was 29%. This low value could be due to the heterogeneous nature of the encapsulated hydrolysates and their chemical incompatibilities with the wall materials. Moreover, Interactions between the hydrolysates and the nanocarriers may not be present or strong enough to keep the hydrolysates within the chitosan alginate matrix. The porosity of the chitosan/alginate matrix leads to leakage of SPH from the matrix, resulting in low EE. Impurities present in the SPH could reduce the strength of electrostatic interactions (Sorasitthiyanukarn et al., 2018, 2019).

3.3. Surface morphology of SPH-loaded CS/AL NPs

Morphological characteristics of the SPH-loaded nanoparticles were evaluated using TEM. Figure 3 shows the TEM images for SPH-loaded CS/AL NPs. There are solid, dense nanoparticles in the suspension, and it could be observed that linkages appeared to be present between the particles. Particles were fairly spherical and distinct but did not possess a smooth surface. Similar patterns have been observed for acetamiprid-loaded and nifedipine-loaded chitosan alginate nanoparticles (Kumar et al., 2015; Li et al., 2008). Particle sizes were smaller at around 50 nm in TEM, which may be explained by differences in the measurement of particle sizes from dynamic light scattering (DLS) and TEM. In DLS, the hydrodynamic size of the particles is measured, which is affected by the agglomeration of the particles. This results in large particle sizes in DLS compared to TEM (Kumar et al., 2015). Agglomeration of nanoparticles may be attributed to the changes in the zeta potential of the particles. Generally, zeta potential below −30 mV or above +30 mV is considered more suitable to avoid agglomeration of the nanoparticles. Hence, SPH-loaded CH/AL nanoparticles could be agglomerated as they have a −30 mV of zeta potential (Moraru et al., 2020).

3.4. Chemical interactions of CS/AL NPs and their precursors

The FTIR spectra for SPH, chitosan, alginate, blank CS/AL NPs, and SPH encapsulated CS/AL NPs are shown in Figure 4. In the chitosan FTIR spectrum, there are a few characteristic peaks. The peaks at 3,358 cm^{-1}, 2,879 cm^{-1}, 1,653 cm^{-1}, 1,567 cm^{-1}, 1,154 cm^{-1}, and 1,061 cm^{-1} demonstrated the overlapping of O-H and N-H stretching, C-H stretching, amide bands of the residual N-acetyl groups, N-H bend of primary amine groups, bridge of -O- stretch and C-O stretch respectively (Mukhopadhyay et al., 2015). Alginate showed characteristic peaks at 1,600 cm^{-1} and 1,408 cm^{-1}, attributed to symmetric and asymmetric stretching from carboxylate salt groups. The band at 1,025 cm^{-1} corresponds to the C-O-C starching vibrations from its saccharide structure (Liu et al., 2018; Mukhopadhyay et al., 2015). In SPH, peaks around 2,900 cm^{-1} correspond to O-H stretching, while the peaks at 1,576 cm^{-1} and 1,510 cm^{-1} are attributed to amide II vibrations, N-H deformation, and C-N stretching. Another distinct

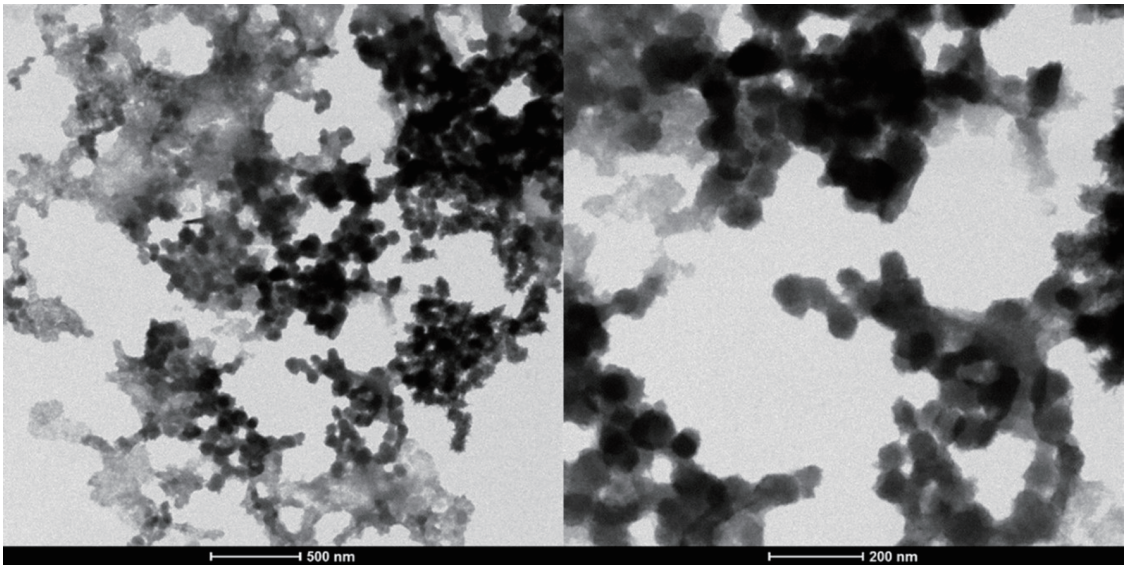

Figure 3. Transmission electron microscopic images for optimized SPH (S. salar by-product-derived protein hydrolysates) encapsulated CH/AL (chitosan/alginate) nanoparticles at two resolutions (500 nm and 200 nm).

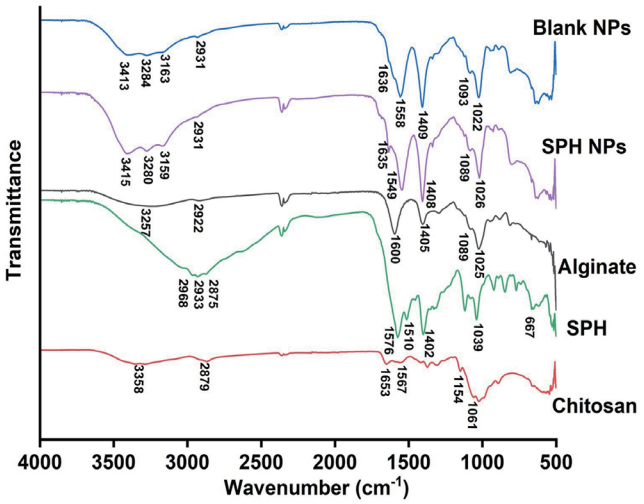

Figure 4. FTIR spectra for chitosan, SPH, alginate, SPH CS/AL NPs, and blank CS/AL NPs. SPH = S. salar by-product-derived protein hydrolysates, CS = chitosan, AL = alginate, NPs = nanoparticles.

peak at 1,402 cm^{-1} related to the amide III stretching vibrations could be observed. Peaks corresponding to C-H starching and N-H bending could be seen at 1,039 cm^{-1} and 667 $cm^{-1,}$ respectively (Sarabandi et al., 2019). In the IR spectrum of CS/AL NPs, peaks corresponding to the amine and carbonyl stretching were moved to 3,413 cm^{-1}. This may be due to the interactions between alginate and chitosan after complexation. Peaks attributed to the symmetric and asymmetric stretching from carboxylate salt groups have shifted to 1,409 cm^{-1} and 1,636 $cm^{-1,}$ respectively (Liu et al., 2018). The peak related to the amino groups also shifted from 1,567 cm^{-1} to 1,558 cm^{-1}. Moreover, amide peaks at 1,653 cm^{-1} were shifted to 1,636 cm^{-1}. These changes reflect the electrostatic interactions between the amino group of chitosan and the carbonyl group of alginates. Amide II bands in the SPH could be overlapped with the shifting of the amino groups of chitosan in SPH-loaded CS/AL NPs (Mukhopadhyay et al., 2015; Sorasitthiyanukarn et al., 2019).

3.5. Changes in nanoparticle crystallinity

X-ray diffractograms for raw materials and nanoparticles are shown in Figure 5. An XRD was used to evaluate the crystalline nature of the raw materials and SPH-encapsulated nanoparticles. Two main characteristic crystalline peaks at 2θ values of 10.26 and 20.04 were observed in the chitosan, reflecting the crystalline nature. X-ray diffractograms of sodium alginate have few characteristic peaks at diffraction angles (2θ values) of 13.94, 21.9, 29.68, and 37.36, which indicate their semi-crystalline nature where broader peaks indicate the amorphous nature of alginate (Kumar et al., 2021; Nikolova et al., 2022; Yan et al., 2017). X-ray diffractogram of SPH exhibited a few peaks at 2θ values of 6.22, 19.44, 22.06, and 32.92 and a broad peak. This depicts that the SPH was not arranged in an orderly manner and had a mostly amorphous structure. Moreover, it reflects that SPH has some crystallinity (Jin et al., 2019; Noman et al., 2020; Wang et al., 2018). When considering the blank CS/AL NPs, it is visible that there are several sharp peaks in the X-ray diffractogram (Figure 5e), indicating the crystalline nature of the particles. These sharp peaks may be due to the presence of $CaCl_2$ in the nanoparticles used to crosslink with alginate (Scolari et al., 2019). SPH-loaded CS/AL NPs also showed several sharp peaks in the X-ray diffractogram, indicating the crystalline nature of the nanoparticles. Some peaks corresponding to SPH have also appeared in the X-ray diffractogram of SPH-loaded CS/AL NPs, indicating the incorporation of SPH into the chitosan and alginate polymer matrix. However, the crystallinity of SPH-loaded CS/AL NPs could be another reason for the lower encapsulation efficiency observed in the nanoparticles. The crystallinity of the nanoparticles prevents the proper exfoliation of SPH in the chitosan-alginate polymer matrix, resulting in lower EE.

In contrast, nanoparticles have been used to encapsulate crystalline molecules to reduce crystallinity and improve their bioavailability. For instance, quercetin has been encapsulated with chitosan and alginate by Nalini et al. with 82% of EE (Nalini et al., 2019). It has been found that the crystallinity of quercetin reduced after the encapsulation. Moreover, the crystallinity of Cucurmin glutaric has reduced after encapsulation in chitosan/alginate nanoparticles (EE of 76%). This indicated the encapsulation of Cucurmin glutaric in the amorphous region in the nanoparticle matrix (Sorasitthiyanukarn et al., 2018).

3.6. Release behavior of SPH-loaded CS/AL NPs in gastrointestinal digestion

The SPH release pattern of the optimized CS/AL nanoparticles under simulated gastrointestinal digestion conditions is shown in Figure 6 as a time continuum. The SPH release under simulated saliva (0–10 min), gastric (30–120 min), and intestinal (120–240 min) digestion conditions were studied. At the end of the saliva digestion, 51% of SPH had been released from the nanoparticles. This could be attributed to the SPH not fully encapsulated in the nanoparticles. As the encapsulation efficiency of the SPH is relatively low (30%), a significant amount of peptide was available in the nanoparticle suspension. It would be readily released in salivary juice. Moreover, SPH that are adsorbed to the chitosan and alginate network by weak interactions may be released easily (Rahaiee et al., 2017).

In the gastric environment, the release rate increased to 73% during the first 30 min, while at the end of the gastric digestion, the release rate was 76% (after 2hrs). Around 25% of SPH was released in the intestinal phase. The SPH release rate in the later digestion compartments was low compared to the initial saliva digestion. The initial burst release may be due to the release of SPH that is adsorbed weakly with the polymer matrix. The later slow release of SPH may be due to the harsh conditions in the gastric environment, such as extreme pH (1.2), and digestive enzymes, and suggests that the encapsulated SPH is protected in the chitosan-alginate polymer matrix. Chitosan is soluble in acidic conditions, while alginate is insoluble. Alginate forms a rigid gel structure with chitosan in acidic conditions, preventing the diffusion of SPH from the polymer matrix (Chen et al., 2019; Rahaiee et al., 2017; Xu et al., 2021). Moreover, the release of the SPH in the gastric phase may depend on the gastric media's ionic strength (Feng et al., 2020; Tan et al., 2017). The protective effects of CS/AL nanoparticles for bioactive compounds observed here in the gastric environment agree with previous studies (Chen et al., 2019; Feng et al., 2020; Tan et al., 2017; Xu et al., 2021). For instance, insulin encapsulated in chitosan and alginate nanoparticles showed 14% insulin release in gastric conditions, suggesting the nanoparticles' stability (Wong et al., 2020).

Intestinal digestion was carried out for 2 hours, and continuous release of SPH was observed. Around 96% of SPH was released

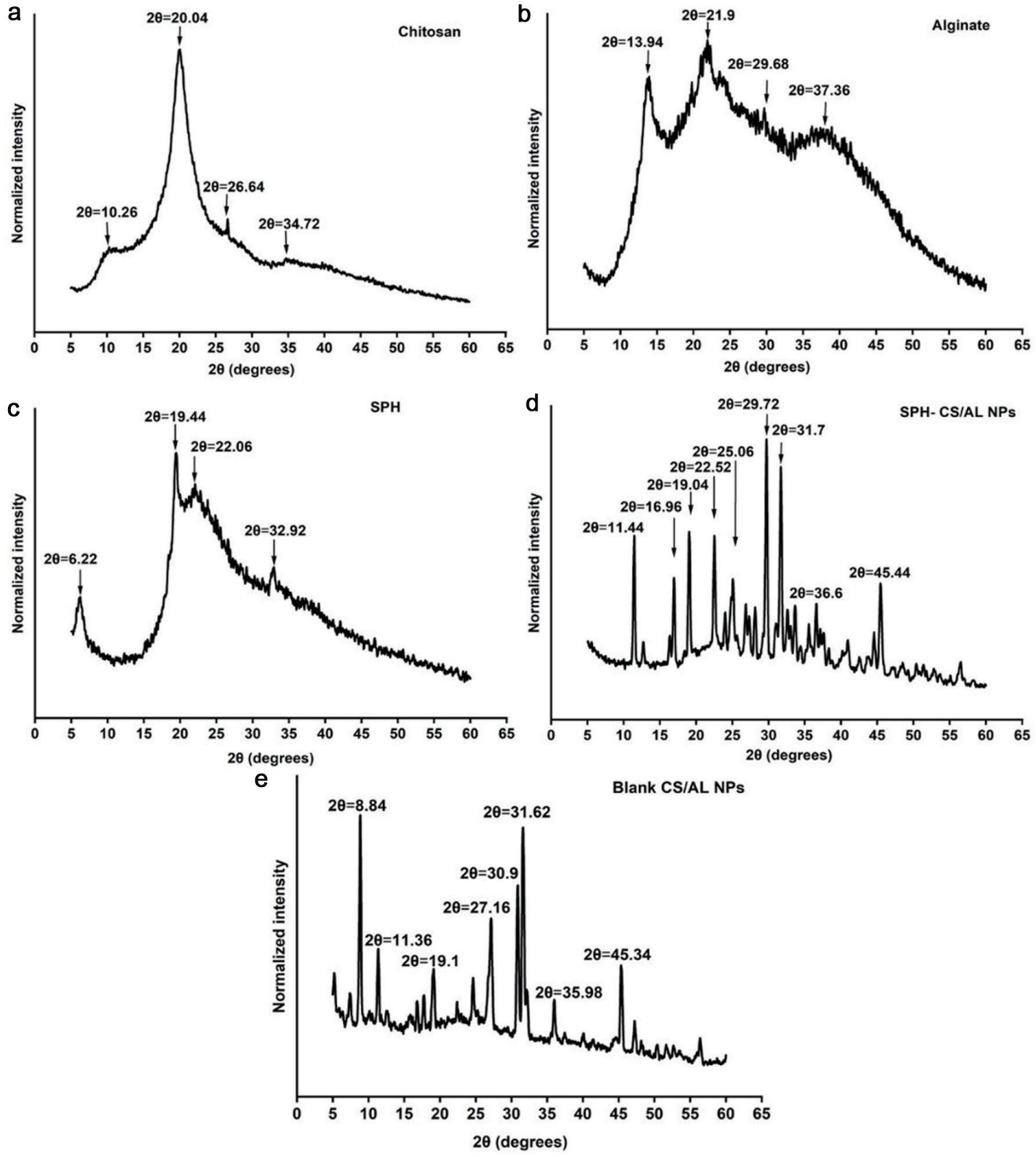

Figure 5. XRD spectra for chitosan (a), alginate (b), SPH (c), SPH-CS/AL NPs (d), and blank CS/AL NPs (e). SPH = S. salar by-product-derived protein hydrolysates, CS = chitosan, AL = alginate, NPs = nanoparticles.

at the end of the digestion process. During gastric digestion, the release of SPH was around 20%. In high pH conditions, swelling of the sodium alginate chain may have occurred, leading to the destruction of the chitosan alginate polymer matrix and the release of the SPH from the intestinal phase. Deprotonation of the chitosan at neutral pH and the weak interactions between the polymers could also result in the release of SPH. Moreover, the ionic strength of the intestinal juice may affect the electrostatic interactions between two polymers, leading to the release of SPH (Chen et al., 2019; Feng et al., 2020). CS/AL nanoparticles were able to release the re-

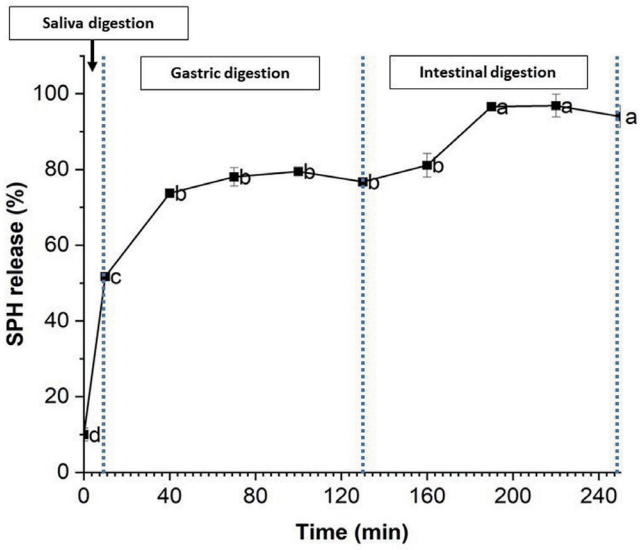

Figure 6. Release % of SPH (S. salar by-product-derived protein hydrolysates) from chitosan/alginate nanoparticles. Mean values with different letters are significantly different ($p < 0.05$).

maining encapsulated SPH in the intestinal phase in a sustainable manner. Sustainable release patterns in the intestinal phase have been obtained for many bioactive compounds encapsulated using CH/AL, including curcumin diethyl diglutarate, polyphenols, resveratrol, insulin, carvacrol, crocin, etc. (Feng et al., 2020; Niaz et al., 2021; Rahaiee et al., 2017; Sorasitthiyanukarn et al., 2018; Tan et al., 2017; Wong et al., 2020).

4. Conclusion

This study aimed to optimize the CH/AL nanoparticles to encapsulate SPH using a Box-Behnken design. It was found that particle size was significantly affected by three independent variables (alginate/chitosan (w/w), alginate/ $CaCl_2$ (w/w), and alginate/peptides (w/w)), and there was an interaction between alginate/chitosan ratio and alginate/SPH ratio. Zeta potential was affected by Alginate/chitosan and alginate/$CaCl_2$ ratios. Meanwhile, encapsulation efficiency was significantly affected by alginate/chitosan and alginate/SPH ratios. However, optimized CS/AL nanoparticles have a relatively low encapsulation efficiency (29%), low particle size (526 nm), and negative zeta potential (−30 mV). XRD and FTIR results affirmed the incorporation of SPH into nanoparticles. SPH-encapsulated CS/AL nanoparticles showed a high release rate in simulated saliva digestion and a sustainable release in the intestinal juice. CS/AL nanoparticles protected the encapsulated SPH from gastric digestion. This study provided preliminary optimized initial steps to encapsulate heterogeneous protein hydrolysates using chitosan and alginate as carriers.

Salmon protein hydrolysate encapsulated nanoparticles can be used in diverse applications across multiple fields. Specially in nutraceuticals and functional foods, these nanoparticles can be used to enhance nutritional value and deliver bioactive peptides with antioxidant, antimicrobial, and anti-inflammatory effects. On the other hand in pharmaceutical applications, its controlled release and therapeutic properties can be used to fabricate pharmaceutical products. Also, there are potential uses for these nanoparticles in biodegradable packaging and biomedical applications such as antimicrobial packaging materials, tissue engineering scaffolds, and implant coatings. These applications leverage the bioactivity, biocompatibility, and enhanced delivery capabilities provided by nanoparticle encapsulation.

Acknowledgments

We would like to thank Dr. Hagar Labouta for providing access to the zeta potential measurement infrastructure.

Funding

This study was funded by the Verschuren Center for Sustainability in Energy and the Environment, NSERC Discovery Grant, NSERC CREATE-CAPTURE Program Trainee Fund, and Canada Foundation for Innovation.

Author contributions

Janani Jayasinghe Mudiyanselage: Conceptualization, Methodology, Investigation, Analysis, Writing-original draft. Thilini Dissanayake Methodology and Analysis. Aishwarya Mohan: Methodology and Analysis. Beth Mason. Funding acquisition, Conceptualization, Supervision, Analysis, Reviewing and Editing, and Project administration. Nandika Bandara. Funding acquisition, Supervision, Analysis, Reviewing and Editing.

References

Aguilar-Toalá, E.J., Quintanar-Guerrero, M.D., Liceaga, A., and Zambrano-Zaragoza, M.L. (2022). Encapsulation of bioactive peptides: a strategy to improve the stability, protect the nutraceutical bioactivity and support their food applications. RSC Adv. 12(11): 6449–6458.

Azevedo, M.A., Bourbon, A.I., Vicente, A.A., and Cerqueira, M.A. (2014). Alginate / chitosan nanoparticles for encapsulation and controlled release of vitamin B 2. Int. J. Biol. Macromol. 71: 141–146.

Bhandari, D., Rafiq, S., Gat, Y., Gat, P., Waghmare, R., and Kumar, V. (2020). A Review on Bioactive Peptides: Physiological Functions, Bioavailability and Safety. Int. J. Pept. Res. Ther. 26(1): 139–150.

Bhunchu, S., Rojsitthisak, P., and Rojsitthisak, P. (2015). Effects of preparation parameters on the characteristics of chitosan–alginate nanoparticles containing curcumin diethyl disuccinate. J. Drug Delivery Sci. Technol. 28: 64–72.

Chandrasekar, V., Coupland, J.N., and Anantheswaran, R.C. (2017). Characterization of nisin containing chitosan-alginate microparticles. Food Hydrocolloids 69: 301–307.

Chen, T., Li, S., Zhu, W., Liang, Z., Zeng, Q., Chen, L., Ge, M.D., Zhu, Y.J., Song, Y., Cheung, P.C.K., Zhang, B.B., Liu, L.M., Chen, T., Li, S., Zhu, W., Liang, Z., and Zeng, Q. (2019). Self-assembly pH-sensitive chitosan/alginate coated polyelectrolyte complexes for oral delivery of insulin. J. Microencapsulation 36(1): 96–107.

Du, Z., Liu, J., Zhang, T., Yu, Y., Zhang, Y., Zhai, J., Huang, H., Wei, S., Ding, L., and Liu, B. (2019). A study on the preparation of chitosan-tripolyphosphate nanoparticles and its entrapment mechanism for egg white derived peptides. Food Chem. 286: 530–536.

FAO. (2022). The State of World Fisheries and Aquaculture 2022. Towards Blue Transformation. FAO, Rome.

Feng, R., Wang, L., Zhou, P., Luo, Z., Li, X., and Gao, L. (2020). Development of the pH responsive chitosan-alginate based microgel for encapsulation of Jughans regia L. polyphenols under simulated gastrointestinal digestion in vitro. Carbohydr. Polym. 250: 116917.

Fisheries and Oceans Canada. (2022). Farmed Salmon. https://www.dfo-

mpo.gc.ca/aquaculture/sector-secteur/species-especes/salmon-saumon-eng.htm.Acessed 16May. 2022.

Flores, F.P., Singh, R.K., Kerr, W.L., Pegg, R.B., and Kong, F. (2014). Total phenolics content and antioxidant capacities of microencapsulated blueberry anthocyanins during in vitro digestion. Food Chem. 153: 272–278.

Flores-Jiménez, N.T., Ulloa, J.A., Silvas, J.E.U., Ramírez, J.C.R., Ulloa, P.R., Rosales, P.U.B., Carrillo, Y.S., and Leyva, R.G. (2019). Effect of high-intensity ultrasound on the compositional, physicochemical, biochemical, functional and structural properties of canola (Brassica napus L.) protein isolate. Food Res. Int. 121: 947–956.

Gao, R., Yu, Q., Shen, Y., Chu, Q., Chen, G., Fen, S., Yang, M., Yuan, L., McClements, D.J., and Sun, Q. (2021). Production, bioactive properties, and potential applications of fish protein hydrolysates: Developments and challenges. Trends Food Sci. Technol. 110: 687–699.

Giroux, H.J., Shea, R., Sabik, H., Fustier, P., Robitaille, G., and Britten, M. (2019). Effect of oil phase properties on peptide release from water-in-oil-in-water emulsions in gastrointestinal conditions. LWT 109: 429–435.

Görgüç, A., Gençdağ, E., and Yılmaz, F.M. (2020). Bioactive peptides derived from plant origin by-products: Biological activities and techno-functional utilizations in food developments – A review. Food Res. Int. 136: 109504.

Honary, S., and Zahir, F. (2013). Effect of Zeta Potential on the Properties of Nano-Drug Delivery Systems - A Review (Part 2). Trop. J. Pharm. Res. 12(2): 265–273.

Hosseini, S., and Varidi, M. (2021). Optimization of Microbial Rennet Encapsulation in Alginate – Chitosan Nanoparticles. Food Chem. 352: 129325.

Ji, M., Sun, X., Guo, X., Zhu, W., Wu, J., Chen, L., Wang, J., Chen, M., Cheng, C., and Zhang, Q. (2019). Green synthesis, characterization and in vitro release of cinnamaldehyde/sodium alginate/chitosan nanoparticles. Food Hydrocolloids 90: 515–522.

Jin, B., Zhou, X., Zhou, S., Liu, Y., Zheng, Z., Liang, Y., and Chen, S. (2019). Nano-encapsulation of curcumin using soy protein hydrolysates – tannic acid complexes regulated by photocatalysis: a study on the storage stability and in vitro release. J. Microencapsulation 36(4): 385–398.

Kumar, D., Kumar, S., Kumar, S., Rohatgi, S., and Kundu, P.P. (2021). Synthesis of rifaximin loaded chitosan-alginate core-shell nanoparticles (Rif@CS/Alg-NPs) for antibacterial applications. Int. J. Biol. Macromol. 183: 962–971.

Kumar, S., Chauhan, N., Gopal, M., Kumar, R., and Dilbaghi, N. (2015). Development and evaluation of alginate-chitosan nanocapsules for controlled release of acetamiprid. Int. J. Biol. Macromol. 81: 631–637.

Li, D., Wei, Z., and Xue, C. (2021). Alginate-based delivery systems for food bioactive ingredients: An overview of recent advances and future trends. Compr. Rev. Food Sci. Food Saf. 20(6): 5345–5369.

Li, P., Dai, Y.N., Zhang, J.P., Wang, A.Q., and Wei, Q. (2008). Chitosan-Alginate Nanoparticles as a Novel Drug Delivery System for Nifedipine. Int. J. Biomed. Sci. 4(3): 221–228.

Liu, J., Xiao, J., Li, F., Shi, Y., Li, D., and Huang, Q. (2018). Chitosan-sodium alginate nanoparticle as a delivery system for ε-polylysine: Preparation, characterization and antimicrobial activity. Food Control 91: 302–310.

Mohan, A., Rajendran, S.R.C.K., Thibodeau, J., Bazinet, L., and Udenigwe, C.C. (2018). Liposome encapsulation of anionic and cationic whey peptides: Influence of peptide net charge on properties of the nanovesicles. LWT–Food Sci. Technol. 87: 40–46.

Moraru, C., Mincea, M., Menghiu, G., and Ostafe, V. (2020). Understanding the Factors Influencing Chitosan-Based Nanoparticles-Protein Corona Interaction and Drug Delivery Applications. Molecules 25(20): 4758.

Mukhopadhyay, P., Chakraborty, S., Bhattacharya, S., Mishra, R., and Kundu, P.P. (2015). pH-sensitive chitosan/alginate core-shell nanoparticles for efficient and safe oral insulin delivery. Int. J. Biol. Macromol. 72: 640–648.

Nalini, T., Basha, S.K., Mohamed Sadiq, A.M., Kumari, V.S., and Kaviyarasu, K. (2019). Development and characterization of alginate / chitosan nanoparticulate system for hydrophobic drug encapsulation. J. Drug Delivery Sci. Technol. 52: 65–72.

Niaz, T., Imran, M., and Mackie, A. (2021). Improving carvacrol bioaccessibility using core–shell carrier-systems under simulated gastrointestinal digestion. Food Chem. 353: 129505.

Nikolova, D., Simeonov, M., Tzachev, C., Apostolov, A., Christov, L., and Vassileva, E. (2022). Polyelectrolyte complexes of chitosan and sodium alginate as a drug delivery system for diclofenac sodium. Polym. Int. 71(6): 668–678.

Noman, A., Ali, A.H., AL-Bukhaiti, W.Q., Mahdi, A.A., and Xia, W. (2020). Structural and physicochemical characteristics of lyophilized Chinese sturgeon protein hydrolysates prepared by using two different enzymes. J. Food Sci. 85(10): 3313–3322.

Perry, S.L., and McClements, D.J. (2020). Recent advances in encapsulation, protection, and oral delivery of bioactive proteins and peptides using colloidal systems. Molecules 25(5): 1161.

Rahaiee, S., Hashemi, M., Shojaosadati, S.A., Moini, S., and Razavi, S.H. (2017). Nanoparticles based on crocin loaded chitosan-alginate biopolymers: Antioxidant activities, bioavailability and anticancer properties. Int. J. Biol. Macromol. 99: 401–408.

Rahaiee, S., Shojaosadati, S.A., Hashemi, M., Moini, S., and Razavi, S.H. (2015). Improvement of crocin stability by biodegradeble nanoparticles of chitosan-alginate. Int. J. Biol. Macromol. 79: 423–432.

Rajendran, S.R.C.K., Mohan, A., Khiari, Z., Udenigwe, C.C., and Mason, B. (2018). Yield, physicochemical, and antioxidant properties of Atlantic salmon visceral hydrolysate: Comparison of lactic acid bacterial fermentation with Flavourzyme proteolysis and formic acid treatment. J. Food Process. Preserv. 42(6): 1–11.

Ramakrishnan, V.V., Hossain, A., Dave, D., and Shahidi, F. (2024). Salmon processing discards: a potential source of bioactive peptides – a review. Food Prod., Process. Nutr. 6(1): 1–32.

Sarabandi, K., Gharehbeglou, P., and Jafari, S.M. (2020). Spray-drying encapsulation of protein hydrolysates and bioactive peptides: Opportunities and challenges. Drying Technol. 38(5–6): 577–595.

Sarabandi, K., Mahoonak, A.S., Hamishehkar, H., Ghorbani, M., and Jafari, S.M. (2019). Protection of casein hydrolysates within nanoliposomes: Antioxidant and stability characterization. J. Food Eng. 251: 19–28.

Scolari, I.R., Páez, P.L., Sánchez-Borzone, M.E., and Granero, G.E. (2019). Promising Chitosan-Coated Alginate-Tween 80 Nanoparticles as Rifampicin Coadministered Ascorbic Acid Delivery Carrier Against Mycobacterium tuberculosis. AAPS PharmSciTech 20(2): 1–21.

Shishir, M.R.I., Xie, L., Sun, C., Zheng, X., and Chen, W. (2018). Advances in micro and nano-encapsulation of bioactive compounds using biopolymer and lipid-based transporters. Trends Food Sci. Technol. 78: 34–60.

Sorasitthiyanukarn, F.N., Muangnoi, C., Bhuket, P.R.N., Rojsitthisak, P., and Rojsitthisak, P. (2018). Chitosan/alginate nanoparticles as a promising approach for oral delivery of curcumin diglutaric acid for cancer treatment. Mater. Sci. Eng. C 93: 178–190.

Sorasitthiyanukarn, F.N., Ratnatilaka Na Bhuket, P., Muangnoi, C., Rojsitthisak, P., and Rojsitthisak, P. (2019). Chitosan/alginate nanoparticles as a promising carrier of novel curcumin diethyl diglutarate. Int. J. Biol. Macromol. 131: 1125–1136.

Tan, P.Y., Tan, T.B., Chang, H.W., Tey, B.T., Chan, E.S., Lai, O.M., Sham Baharin, B., Nehdi, I.A., and Tan, C.P. (2017). Effects of Environmental Stresses and in Vitro Digestion on the Release of Tocotrienols Encapsulated Within Chitosan-Alginate Microcapsules. J. Agric. Food Chem. 65(48): 10651–10657.

Wang, L., Ding, Y., Zhang, X., Li, Y., Wang, R., Luo, X., Li, Y., Li, J., and Chen, Z. (2018). Isolation of a novel calcium-binding peptide from wheat germ protein hydrolysates and the prediction for its mechanism of combination. Food Chem. 239: 416–426.

Wong, C.Y., Al-Salami, H., and Dass, C.R. (2020). Formulation and characterisation of insulin-loaded chitosan nanoparticles capable of inducing glucose uptake in skeletal muscle cells in vitro. J. Drug Delivery Sci. Technol. 57: 101738.

Xu, Z., Chen, L., Duan, X., Li, X., and Ren, H. (2021). Microparticles based on alginate/chitosan/casein three-dimensional system for oral insulin delivery. Polym. Adv. Technol. 32(11): 4352–4361.

Yan, J., Huang, Y., Chrisey, D.B., Jorgensen, M., Gibbons, A., Sui, K., and Aprilliza, M. (2017). Characterization and properties of sodium algi-

nate from brown algae used as an ecofriendly superabsorbent. IOP Conf. Ser.: Mater. Sci. Eng. 188(1): 012019.

Zamora-Sillero, J., Gharsallaoui, A., and Prentice, C. (2018). Peptides from Fish By-product Protein Hydrolysates and Its Functional Properties: an Overview. Mar. Biotechnol. 20(2): 118–130.

Zhang, L., and Kosaraju, S.L. (2007). Biopolymeric delivery system for controlled release of polyphenolic antioxidants. Eur. Polym. J. 43(7): 2956–2966.

Zimet, P., Mombrú, Á.W., Faccio, R., Brugnini, G., Miraballes, I., Rufo, C., and Pardo, H. (2018). Optimization and characterization of nisin-loaded alginate-chitosan nanoparticles with antimicrobial activity in lean beef. LWT–Food Sci. Technol. 91: 107–116.